Is Pressure the Key to Hydrogen Ordering Ice IV?

Alexander Rosu-Finsen* and Christoph G. Salzmann

Department of Chemistry, University College London, 20 Gordon Street, London WC1H 0AJ, United Kingdom

*Corresponding author: a.rosu-finsen@ucl.ac.uk

Abstract

Hydrochloric-acid-doped ice IV prepared at increasing pressures leads to growing endotherms observed with ambient pressure calorimetry. The endotherms are irreversible leading to three possible scenarios for their origins: (1) a weakly hydrogen-ordered counterpart to ice IV is formed, but ambient pressure favours hydrogen-disordered ice IV, (2) increased pressure creates increased strain within the crystal structure of the ice, which is released upon heating yielding the endotherms or (3) the endotherms are kinetic overshoot effects related to the underlying orientational glass transition. However, X-ray diffraction cannot distinguish between these scenarios. Recent controversies regarding the preparation of ice IV are also discussed.

Introduction

Through a combination of applying pressure and changing the temperature, the polymorphic nature of ice can be explored as shown in the phase diagram in Figure 1(a). Currently, we know of 19 unique phases of ice[1-5] while new polymorphs are waiting to be discovered. The known phases of ice are either hydrogen-ordered/disordered pairs, emptied clathrate hydrates, superionic, or fully dissociated H_2O.[1] Up to pressures of about 50 GPa, the phase diagram is dominated by the hydrogen-ordered/disordered phases. Upon cooling hydrogen-disordered phases, reorientation dynamics allow the hydrogen-bonded H_2O molecules to adopt the most favourable orientations, thus forming the hydrogen-ordered phases. Such hydrogen-ordering occurs spontaneously in ices III/IX and VII/VIII with decreasing temperature while dopants are required to order ices I*h*, V, VI, and XII to ices XI, XIII, XV, and XIV, respectively. Only hydrogen-ordered ice II, hydrogen-disordered ice IV, and the emptied clathrate hydrates of ices XVI and XVII lack their respective counterparts.

Spurred on by Tammann's suspicion of a metastable phase,[6] Bridgman discovered the phase that we now call ice IV.[7] Ice IV can be made in a narrow pressure window, 0.500 – 0.535 GPa, by slow decompression of ice VI,[8] however, such formation has proven to be sporadic.[9] Instead, consistent ice IV formation has been shown through the use of organic nucleating agents from the liquid,[10, 11] as well as slow heating of high-density amorphous (HDA) ice at 0.81 GPa.[12, 13] Increasing the heating rate leads to increasing amounts of ice XII where fast heating rates result in phase-pure ice XII.[14] Pressure is also important in ice IV formation, increased pressures above 0.81 GPa also leads to greater amounts of ice XII being formed[15] as ice XII is a persistent metastable phase of ice when subjected to a wide range of pressures.[16]

The rhombohedral structure of ice IV is composed of 16 H_2O molecules per unit cell with an *R*-3*c* space group.[16, 17] Figure 1(b) shows the crystal structure of ice IV featuring layers of six-

membered, chair conformation rings in cyan which are penetrated by hydrogen bonds in yellow. As seen in Figure 1(b), a relation to the structure of ice I*h* can be distinguished, and as such, the Engelhardt-Kamb collapse was proposed for how an ice I*h*-type structure can lead to a structure with an ice IV topology through compression.[17] This collapse can be thought of as one ice I*h* layer breaking the hydrogen bonds to the above- and below-layers. These broken connections reconnect through hydrogen-bonding to the two layers above and below thereby forming the interpenetrating bonds. However, with increasing pressure ice IV is not made directly from ice I*h*, but through HDA which is created *via* pressure-induced amorphization.[18] The reason for ice I*h* not following the Engelhardt-Kamb collapse to completion is the presence of hydrogen disorder in ice. The chances of breaking and reforming a hydrogen-bond, successfully, is 50% due to the disorder. This is why HDA was termed a derailed state when attempting to compress ice I*h* into ice IV.[19] With a structure containing no hydrogen-order/disorder, such as NH_4F which is isostructural with ice I, a crystalline NH_4F-II is made through isothermal compression.[19] Interestingly, NH_4F-II is isostructural with ice IV and ice IV environments have been detected in HDA through molecular dynamics simulations,[20] lending credence to the idea that HDA is indeed a derailed state along the ice I*h* to IV compression pathway.

As shown by the "question mark" below ice IV in Figure 1(a), the hydrogen-ordered counterpart is currently unknown but weak calorimetric signs of its potential existence have been described in ref. 21. To both study the ice IV system and hunt for its ordered counterpart neutron diffraction, calorimetry, IR and Raman spectroscopy techniques have been used to investigate ice IV.[12, 21, 22] In calorimetry a disordering endotherm upon heating (and ordering exotherm upon cooling) is seen in 0.01M HCl-doped ice V/XIII and VI/XV[23-25] which indicates the reversible transformation of phases. A small endotherm, potentially disordering a hydrogen-ordered ice IV into hydrogen-disordered ice IV, has been noted with the same dopant,[21] however, diffraction of such ice has not yielded any information about a new ordered structure. The key question is if the endotherm takes up latent heat or if it is an overshoot-feature connected to the underlying glass transition of the unfreezing of the molecular reorientations.[26]

Investigating ice-polymorphs at different pressures has led to some interesting new insights. Ice VII/VIII displays changing kinetics with respect to hydrogen-ordering at increased pressures during its phase transition.[27] The deep glassy states of ice VI were discovered at increasing pressures,[26, 28] ultimately leading to the latest phase, ice XIX,[5] which is a distorted version of the hydrogen-disordered ice VI. However, it has also been suggested that ice XIX is a new hydrogen-ordered phase of ice VI.[3, 4] Calorimetric measurements of high-pressure HCl-doped ice V/XIII has shown the emergence of a transient ordering regime[29] similar to what is observed for ice XIX/VI. Further experiments aiming at increasing the pressure on the ice V/XIII system could produce a deep glassy state of ice V, and yet another crystallographically unique phase of ice. The effect of increased pressure on ice IV has not been explored. In this work, we intend to begin this exploration with powder X-ray diffraction and calorimetry of metastable 0.01 M HCl-doped ice IV samples annealed at high pressures.

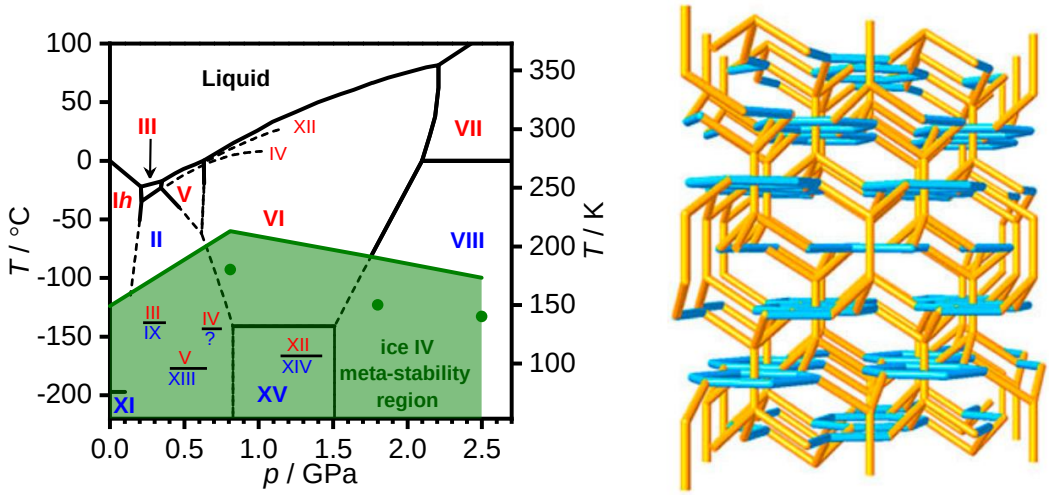

Figure 1: (a) The phase diagram of H_2O including the low-temperature metastability region of ice IV in green, and the bold green spheres highlighting the pressures at which ice IV was annealed to before extraction at ambient pressure for further analysis. (b) The hydrogen-bonded network of ice IV with the interpenetrated six-membered rings highlighted in cyan.[1]

Experimental

Preparation of doped ice IV samples

For the preparation of doped ice IV samples, 0.01 M HCl (Sigma Aldrich) was pipetted into an indium cup inside a pressure die precooled to 77 K with liquid nitrogen. Depending on the final pressure, different volumes and pressure dies were used; 300 μL 0.01 M HCl were pipetted into a cooled 8 mm diameter pressure die for the 0.81 and 1.80 GPa experiments. For the 2.5 GPa experiments, 50 μL 0.01 M HCl were pipetted into a precooled 5 mm diameter pressure die. Initially, the ice was compressed to 1.6 GPa forming HDA, followed by decompression to 0.81 GPa in a Z100 Zwick Test Machine (Zwick/Roell Group, GmbH). At this pressure the HDA was heated at <0.4 K min^{-1} from 77 K until a volume change was observed indicating ice IV formation. Following the heating step, the 0.81 GPa ice IV sample was slow-cooled at 2.5 K min^{-1} to 77 K and extracted at ambient pressure for further analysis. For the high-pressure samples, however, the pressure was further increased from 0.81 GPa to 1.8 or 2.5 GPa at 77 K followed by heating and subsequent slow-cooling at 2.5 K min^{-1} before extraction in a liquid nitrogen environment. To compare against pure ice IV, a pure pressure-quenched ice IV sample at 0.81 GPa was also made following the same steps as mentioned above. Additionally, a 0.01 M LiOH-doped ice IV sample was prepared at 0.81 GPa.

The Zwick Test Machine is equipped with a force sensor that works up to 100 kN. The pressures in the samples were estimated by dividing the measured forces by the cross-sectional areas of the bores of the piston cylinders. The indium linings are used to reduce frictional forces within the piston cylinders. Through comparison with phase-transition pressures from the literature the pressures reported here are estimated to be accurate within 0.02 GPa.

Powder X-ray diffraction

Powders of the recovered ice IV samples were transferred under liquid nitrogen into a purpose-built Kapton-window sample holder mounted on a Stoe Stadi P diffractometer with Cu $K_\alpha 1$

radiation at 40 kV, 30 mA and monochromated by a Ge 111 crystal. Data were collected using a Mythen 1 K linear detector, and the temperature of the samples was maintained at 95 K with an Oxford Instruments CryojetHT.

Differential scanning calorimetry

Small pieces of ice IV were transferred into stainless-steel capsules with screwable lids under liquid nitrogen. These were quickly transferred into a precooled Perkin Elmer DSC 8000 advanced double-furnace differential scanning calorimeter with a base temperature of 93 K. Thermograms were recorded upon heating to 136 K at 10 K min^{-1} followed by cooling back to 93 K at 5 K min^{-1}. The samples were then reheated at 10 K min^{-1} from 93 to 263 K, and the previous heating/cooling procedure was repeated with the resulting ice I*h*. Glass transition investigations were conducted by heating the ice from base to 263 K at 10 K min^{-1}, but also by annealing the ice (for 0, 1, and 2 hours) at 125 K before cooling back to base temperature and reheating to 263 K. The moles of ice in the DSC capsules were determined by recording the endothermic melting of ice at 0 °C and using 6,012 J mol^{-1} as the enthalpies of melting of H_2O ice I*h*. The thermograms of ice I*h* were subtracted from the previously recorded data as a background correction. The resulting DSC signal was divided by the number of moles of H_2O and the heating/cooling rate which yields a quantity with J mol^{-1} K^{-1} as the unit.

Results

To investigate the effect of pressure on ice IV and its potential hydrogen-ordering phase transition, the low-temperature region of metastability was mapped first. Figure 2(a) shows the phase transitions as HDA is heated at 0.81 GPa forming ice IV at about 162 K which is further transformed to ice VI/XV at about 213 K. The same pressure profiles are shown for higher pressure ice IV samples heated at 1.8 and 2.5 GPa. Their transitions into ice VI at 190 K and VIII at 173 K, respectively, yields the upper limit of stability as shown with the bold green line in Figure 1(a). To extend this metastability line to 0 GPa (or ambient pressure), literature data[30] of the ice IV → ice I*sd* transition at ~149 K was used which is latter corroborated by the calorimetric data presented in this work. As ice IV is denser than HDA, a negative change in volume is observed. The same is the case for ices VI and ice VIII which are denser than ice IV, hence the densification. Regarding the formation of ice IV, differing opinions can be found in the literature. Considering its "will-o-the-whisp" nature,[9] ice IV can be difficult to make and minor impurities of ice XII are commonplace. With a heating rate of <0.4 K min^{-1}, HDA decompressed to ambient pressure, and then re-compressed to 0.81 GPa forms a 95% ice IV (with 5% ice XII).[13] Later experimental work mentions that the importance of the heating rate as not being crucial.[15] Instead, how the ice is treated with respect to pressure is more important. In ref. 15 the HDA is decompressed to a desired pressure, such as 0.8 GPa, but not to ambient pressure before recompression as in ref. 13. Through this compression program, a 62% "pure" ice IV was created with a heating rate of 0.5 K min^{-1}. It was therefore speculated that the HDA decompressed to ambient pressure forms cracks within the ice. These cracks act as nucleating sites aiding in the formation of a purer ice IV when the HDA with cracks is heated slowly.[15]

The ice IV analysed in this work was made by decompression of HDA directly to 0.81 GPa, not ambient pressure, and heated at <0.4 K min^{-1} as shown in Figure 2(b). This means, according to ref. 15, the ice IV-promoting cracks should not be present, and a less pure ice IV

should be the result. However, the purity of ice IV analysed with XRD and shown in figure 2(c) is akin to that of ref. 13 containing only a few percent ice XII contamination (96% ice IV and 4% ice XII at 0.81 GPa). The present work therefore supports the initial proposal where the heating rate is of utmost importance. In ref. 15, only the average heating rate was quoted. In our experience, it is essential that no active electrical heating element is used which may temporarily lead to high heating rates. In ref. 13, similar to this work, a membrane pump is connected to a LN_2 reservoir through a copper coil surrounding the pressure die. By controlling the pumping speed, the flow of LN_2 through the copper coil is controlled, and therefore so is the change in temperature as shown in Figure 2(b). In ref. 15 a PID-controlled heater may have been used. Such a heater can produce bursts in the heating rate which, when averaged over a long time, appear to be a slow heating rate. However, if such temperature rises occur during the HDA → ice IV transition, ice XII can form instead of ice IV. This could explain the observation of 62% ice IV in ref. 15 instead of much purer ice IV seen in Figure 2(c).

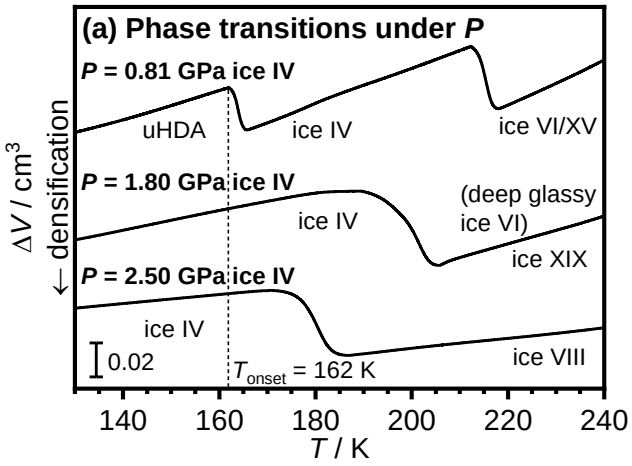

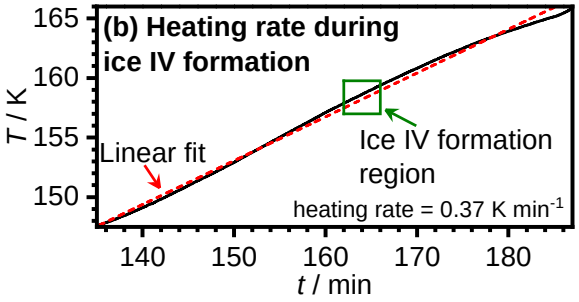

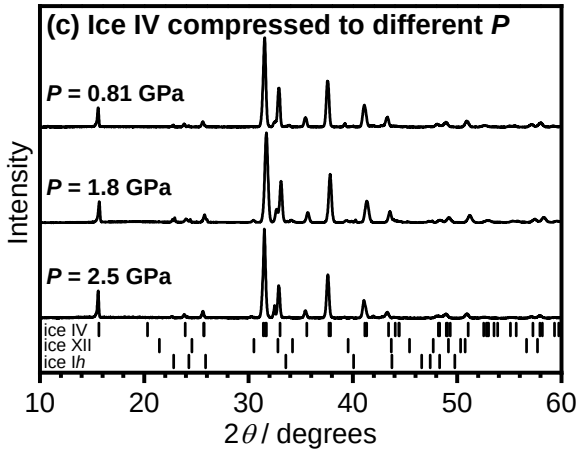

Figure 2: (a) Upon heating HDA at 0.4 K min^{-1} at 0.81 GPa, the onset of the phase transition to ice IV occurs near 162 K. To compress ice IV to 1.80 and 2.50 GPa, ice IV made at 0.81 GPa was pressure-quenched to 77 K before the pressure was increased to the desired value and the ice was reheated. Heating through the ice IV → ice IV/XIX/VIII phase transitions while under pressure leads to the upper temperature limits of the low-temperature ice IV metastability region. (b) illustrates the typical heating rate during ice IV formation in these experiments where the experimental data in black has been fitted with a straight dashed line in red. (c) Powder X-ray patterns of ice IV compressed to the indicated pressures before decompression and analysis at ambient pressure. The tickmarks indicate calculated Bragg reflections of ices IV, XII, and Ih.

Aside from the purity aspects of the ice IV samples shown in Figure 2(c), comparing the diffractograms of the different high-pressure ices is important for this work. With the idea of pressure aiding hydrogen-ordering, new Bragg features should be present at higher pressures if a hydrogen-ordered ice IV is made. Upon close inspection, no such new features can be found as the pressure increased from 0.81 through 1.8 to 2.5 GPa. Also, the peak widths at half maximum remain constant for the ices made at the different pressures. X-ray diffraction is not sensitive to the small electron density of hydrogen atoms. However, if a large degree of hydrogen-ordering is present, the oxygen lattice can be distorted as the space group changes to that of the hydrogen-ordered phase which has been shown to be observable with X-ray diffraction.[23, 31]

The calorimetry of ice IV annealed at different pressures tells a more complex story. Figure 3 shows the thermograms (panel a) and the areas of the observed endotherms up heating (panel b).

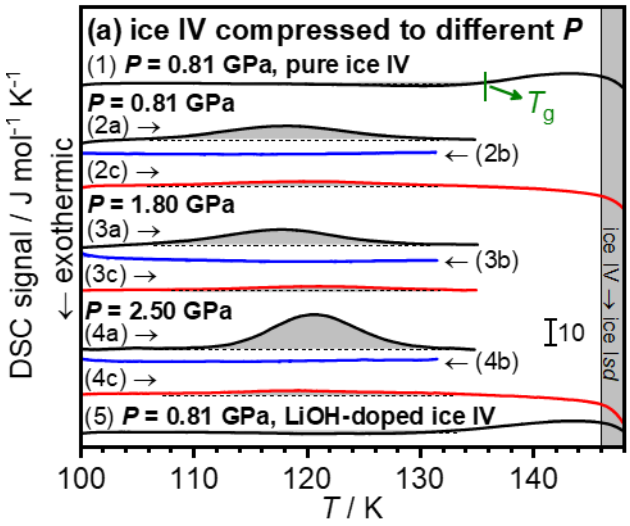

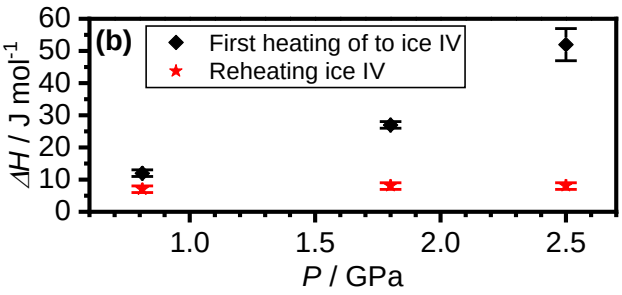

Figure 3: (a) Thermograms of doped ice IV samples heated at ambient pressure. (b) Integrated area of the endotherms, i.e. the ΔH.

Beside the effect of annealing pressure on the ice IV, Figure 3(a) also shows the effect the HCl dopant has on this ice system. The pure ice IV thermogram (labelled 1) is flat until the a shallow exotherm is seen before the T_g labelled in green in figure 3(a) giving rise to an endothermic step leading straight into the ice IV → I*sd* transition.[30] This transition, starting near 149 K, has an associated enthalpic change of 1,137 ± 46 J mol^{-1} which is slightly higher than previous measurements.[30] The arrows for thermograms 2, 3, and 4 indicate the direction of heating with (a) being the first heat, (b) cooling at 5 K min^{-1}, and (c) being the reheat of ambient pressure cooled ice IV. The same thermograms are shown for 1.8 (3a, b, c) and 2.5 GPa (4a, b, c) ice IV samples. The endotherms of (2a) and (2b) resemble previously noted endotherms of HCl-doped ice IV made at 0.81 GPa.[21] With increasing pressure, the first-heat endotherms and their associated integrated areas increase as shown in Figure 3b of the black diamonds. Increasing enthalpies usually indicated increasing hydrogen-ordering as seen when reheating ices V/XIII and VI/XV at ambient pressure,[23, 24] however, the thermograms (2a, 3a, and 4a) are of the first heating and entropy changes can therefore not necessarily be calculated. To be specific, the reversibility of the phase transition needs to be demonstrated which means that an exothermic phase transition is required upon cooling.[23, 24] However, no such hydrogen-ordering exotherm is observed in traces 2b, 3b, and 4b indicating that little or no hydrogen ordering is restored upon ambient pressure cooling. As no difference is noticeable between the cooling thermograms, the reheated thermograms are expected to exhibit small or no disordering endotherms as seen in 2c, 3c, and 4c and clearly shown with red stars in panel (b) of the ΔH values. Only these reheated thermograms can be used to calculate a corresponding percentage of Pauling entropy which equals about 2%. This fraction of Pauling entropy is the same for all the ices prepared at different pressures but analysed at ambient pressure as the ΔH of the red stars shown in panel (b) are similar. The Pauling entropy indicates the anticipated change in entropy during a phase transition from a fully hydrogen-ordered ice to its hydrogen-disordered counterpart.[32] A shift in the data of the 2.5 GPa thermogram is noticeable compared to the lower pressure thermograms which may be an effect of the higher pressure applied to this ice. In previous work, LiOH-doped ice V was analysed and shown to successfully aid in the formation of ice XIII.[23, 29] A 0.81 GPa, 0.0 1M LiOH-doped ice IV sample was therefore made and analysed as shown in thermogram 5 in Figure 3(a). But, similar to LiOH-doped ice VI, this dopant does not aid in hydrogen-ordering as this thermogram looks similar to the pure H_2O ice IV thermogram.[23]

The question now turns to the origins of the endotherms of the first heats. The X-ray diffraction data shows no conclusive evidence of hydrogen-ordering with increasing pressure. The

crystallographic *c*/*a* ratios using the hexagonal unit cell of ice IV were determined from the X-ray diffraction patterns shown in Figure 2(c). These did not show any changes with pressure outside the margins of error. The specific *c*/*a* values are 1.9532 ± 0.0041 at 0.81 GPa, 1.9532 ± 0.0023 at 1.8 GPa and 1.9517 ± 0.0021 at 2.5 GPa. However, X-ray diffraction is not very sensitive to hydrogen-ordering. The first heats of the growing endotherms with increasing pressure may be due to weak ordering. However, ambient pressure ordering after slow-cooling is negligible as seen through calorimetry.

A similar calorimetric behaviour is seen for ice XIV which produces endotherms upon first heating thermograms.[31, 33] However, the areas of the reheated thermograms are much smaller indicating lesser degrees of ordering. KOH-doped ice V has previously been shown to produce endotherms much greater than expected for pure ice V.[34] This large endotherm was initially believed to be due to hydrogen-ordering in ice V, and potentially supported through spectroscopy.[35] It was only when ice XIII was discovered that HCl-doped ice V (ice XIII) could be compared directly to KOH-doped ice V.[36, 37] From these studies it was determined that KOH doping does not lead to significant ordering compared to what is already allowed in pure ice V, *i.e.* the increased endotherm did not relate to hydrogen ordering. These findings are also supported through the changes in lattice constants for the ice XIII to ice V phase transition.[29] Recently, the discovery of a low-temperature endotherm associated with HCl-doped ice VI was mentioned as being due to a more and/or differently ordered ice XV.[38] However, through extensive calorimetry, diffraction, and spectroscopic studies this notion has now been questioned and the new endotherm has been shown to be due to a deep glassy state of ice VI.[5, 26, 28]

The endotherms noted in this work are the largest for ice IV seen to date. Assuming that the endotherms relate entirely to latent hydrogen disordering would mean a ~10% hydrogen-ordered HCl-doped ice IV is formed at 2.5 GPa which would be highest degree of order observed in ice IV so far. However, it needs to be stressed that this is an absolute upper limit, and the actual entropy change may be close to zero. As mentioned earlier, the endotherm may also be understood in terms of an overshoot feature of the underlying orientational glass transition. Due to the lower temperature of the endotherm for the HCl-doped sample compared to the orientational glass transition of pure ice IV, it can be stated that HCl-doping enhances the reorientation dynamics in ice IV. An alternative origin for the endotherms could be due to the strain contained within the ice due to the large pressures applied during ice formation and annealing at high pressure. This stress will not be easily noticeable through diffraction, but the release of the stress upon heating may be noticeable in calorimetry. Raman spectroscopy is also sensitive to stress and strain contained within a crystal structure,[39] and as such, this technique cannot distinguish easily between the effects of strain and hydrogen ordering. *In situ* neutron diffraction under pressure of HCl-doped ice IV will be key to answering the question of how pressure affects the hydrogen ordering of this material.

The idea that pressure aids the hydrogen-ordering of ice IV is applicable if the ordered counterpart has a smaller unit-cell volume compared to the disordered ice IV. As such, higher pressure will lead to greater ordering into a denser ordered structure. Decompression could have adverse effects on the ordering as well, however, the possible extents of this cannot be explored with the current data shown here. A comparison between *in situ* and *ex situ* measurements will shed light on this question.

Considering the structure of ice IV's self-interpenetrating network, it is interesting to speculate if its hydrogen-ordered counterpart would be ferroelectric or antiferroelectric. Ferroelectrically ordered ice was first mentioned for KOH/KOD doped ice I,[40] but has since been challenged.[41] While ice XV is antiferroelectric due to its *P*-1 space group,[42] its two independent H_2O network are actually polarised albeit in opposite directions making it antiferroelectric overall. The same situation is found for the antiferroelectric ice VIII. Overall, there seems to be a strong tendency for ice to hydrogen order in an antiferroelectric fashion.

Ice IV only consists of one hydrogen-bonded network forming interpenetrating hydrogen bonds through six-membered rings as mentioned previously. Using the hexagonal representation of the unit cell, which has a volume three times larger than the corresponding rhombohedral cell, each layer has two interpenetrating hydrogen bonds within the unit cell pointing in the *c* direction. For antiferroelectic ordering, these two hydrogen bonds would have to point in the opposite directions. In the neighbour cells, the directions would have to be opposite meaning that an antiferroelectric hydrogen-ordered ice IV would require a very large unit cell. It can be speculated that this difficulty lies at the origin of the difficulties in preparing hydrogen-ordered ice IV.

Figure 4 compares pressure-quenched ice IV to the HCl-doped ice IV. The exothermic undershoot seen in Figure 3(a) and in the literature[30] forms upon heating without annealing before the endothermic step as the cooling rate during sample preparation is greater than the heating rate during analysis.[43] The reversibility of the glass transition has been explored previously,[30] but the changes in T_g and ΔC_p seen in figure 4 were not observed as annealing time and temperature were not explored. The ΔC_p for pure unannealed ice IV is ~1.6 J mol^{-1} K^{-1} in this work which is slightly larger than the literature of 1.2 J mol^{-1} K^{-1}.[32] Further to this, the onset temperature for the endothermic step in literature is about 140 K when heated at 30 K min^{-1} compared to the orientational T_g in this work of about 136 K when heating at 10 K min^{-1}. These differences can be accounted for as being due to the difference in heating rates between this work and the literature. Another complication is that no plateau region is seen between the heat capacity increase of the orientation glass transition and the onset of the exothermic transition to ice I*sd*. As the ice is annealed at 125 K the undershoot disappears indicating its irreversibility.[30] Along with this disappearance and as expected according to glass transition theory, the T_g shifts to a lower temperature of 132 K. Increasing the annealing time at 125 K shifts the T_g lower again from 129 K to 128 K after 1 and 2 hours of annealing, respectively. Further to this, the exothermic step increases to 2.4 J mol^{-1} K^{-1}, double the value seen in the literature when unnealed.[30] This increase in ΔC_p is expected as the heat capacity increase becomes further separated from the exotherm to ice I*sd*. However, it is important to recall that these endothermic steps are incomplete. A clear plateau is not observed for ice IV, as is also the case for LDA,[21] and therefore a concrete ΔC_p value cannot be given. Conversely, the other metastable phase of ice, ice XII, produces a clear plateau as seen clearly in refs 30, 44.

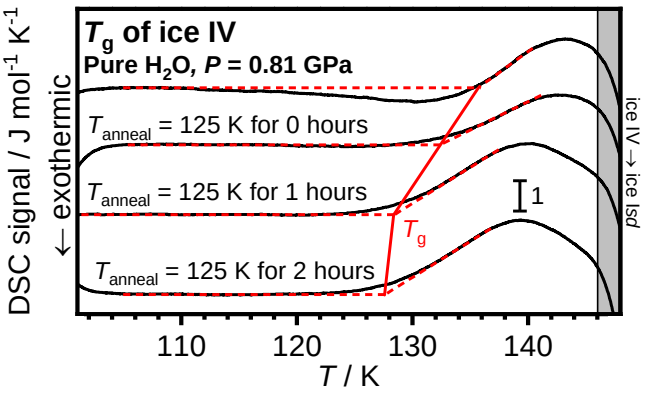

Figure 4: Effect of annealing on the T_g of pure ice IV made at 0.81 GPa. With heating rates of 10 K min^{-1}, the pure ice IV was heated to ice Isd or annealed at 125 K for the indicated times before reheating from base temperature. The solid red line shows the T_g of ice IV as it decreases with increasing annealing time.

Conclusions

Hydrogen ordering ice IV seems difficult as this work has shown. The HCl dopant clearly influences the calorimetric data as seen simply by heating the ice. However, the resulting endothermic features are irreversible and may be due completely or at least in part to other origins than hydrogen disordering. Based on geometry reasons, it may be difficult to achieve antiferroelectric ordering in ice IV which may ultimately be the reason for the difficulties in hydrogen-ordering ice IV.

The increased pressures at which ice IV was made in this study clearly show changes in the calorimetric responses. To date, the greatest ΔH area when heating ice IV at ambient pressure is shown in this work. However, with increased pressure comes the possibility of imparting a certain degree of stress and strain into the crystal structure from the preparation stage. X-ray diffraction may not pick up such effects, but the degree of potential hydrogen-ordering in these ices is not great enough to produce Wyckoff splitting from distortions of the oxygen lattice. Pressure is, however, an interesting aspect when searching for the ordered counterpart to ice IV. If the unit cell volume of ordered ice IV is smaller than that of disordered ice IV, increased pressure will aid in ordering. With this said, there may also be the aspect of decompression effects and how pressure-release affects a potentially ordered ice IV structure. It is possible that much of the gained ordering from pressure reverts to disordered ice IV upon decompression. At present, it seems that ice IV has transformed some of its will-o'-the-wisp character to its hydrogen-ordered counterpart.

Acknowledgements

We thank M. Vickers for help with the X-ray diffraction measurements and J. K. Cockcroft for access to the Cryojet. This project has received funding from the European Research Council

(ERC) under the European Union's Horizon 2020 research and innovation programme (Grant Agreement No. 725271).

Declaration of Interest

The authors declare no conflicts of interest.

References

1. Salzmann, C. G., *J. Chem. Phys.* **2019,** *150*, 060901.
2. Millot, M.; Coppari, F.; Rygg, J. R.; Correa Barrios, A.; Hamel, S.; Swift, D. C.; Eggert, J. H., *Nature* **2019,** *569*, 251-255.
3. Yamane, R.; Komatsu, K.; Gouchi, J.; Uwatoko, Y.; Machida, S.; Hattori, T.; Ito, H.; Kagi, H., *Nat. Commun.* **2021,** *12*, 1129.
4. Gasser, T. M.; Thoeny, A. V.; Fortes, A. D.; Loerting, T., *Nat. Commun.* **2021,** *12*, 1128.
5. Salzmann, C. G.; Loveday, J. S.; Rosu-Finsen, A.; Bull, C. L., *Nat. Commun.* **2021,** *12*, 3162.
6. Tammann, G., *Ann. Phys.* **1900,** *2*, 1-31.
7. Bridgman, P. W., *J. Chem. Phys.* **1935,** *3*, 597-605.
8. Nishibata, K., *Jpn. J. Appl. Phys.* **1972,** *11*, 1701-1708.
9. Ball, P., *H_2O A Biography of Water*. Weidenfeld & Nicolson: 1999.
10. Evans, L. F., *J. Appl. Phys.* **1967,** *38*, 4930-4932.
11. Engelhardt, H.; Whalley, E., *J. Chem. Phys.* **1972,** *56*, 2678-2684.
12. Salzmann, C. G.; Kohl, I.; Loerting, T.; Mayer, E.; Hallbrucker, A., *J. Phys. Chem. B* **2003,** *107*, 2802-2807.
13. Salzmann, C. G.; Loerting, T.; Kohl, I.; Mayer, E.; Hallbrucker , A., *J. Phys. Chem. B* **2002,** *106*, 5587-5590.
14. Salzmann, C. G.; Loerting, T.; Kohl, I.; Mayer, E.; Hallbrucker, *Can. J. Phys.* **2003,** *81*, 25-32.
15. Stern, J.; Loerting, T., *Sci. Rep.* **2017,** *7*, 3995.
16. Klotz, S.; Hamel, G.; Loveday, J. S.; Nelmes, R. J.; Guthrie, M., *Z. Kristallogr.* **2003,** *218*, 117-122.
17. Engelhardt, H.; Kamb, B., *J. Chem. Phys.* **1981,** *75*, 5887-5899.
18. Mishima, O.; Calvert, L. D.; Whalley, E., *Nature* **1984,** *310*, 393-395.
19. Shephard, J. J.; Ling, S.; Sosso, G. C.; Michaelides, A.; Slater, B.; Salzmann, C. G., *J. Phys. Chem. Lett.* **2017,** *8*, 1645-1650.
20. Martelli, F.; Giovambattista, N.; Torquato, S.; Car, R., *Phys. Rev. Mat.* **2018,** *2*, 075601.
21. Salzmann, C. G.; Radaelli, P. G.; Slater, B.; Finney, J. L., *Phys. Chem. Chem. Phys.* **2011,** *13*, 18468-18480.
22. Engelhardt, H.; Whalley, E., *J. Chem. Phys.* **1979,** *71*, 4050-4051.
23. Rosu-Finsen, A.; Salzmann, C. G., *J. Chem. Phys.* **2018,** *148*, 244507.
24. Shephard, J. J.; Salzmann, C. G., *Chem. Phys. Lett.* **2015,** *637*, 63-66.
25. Salzmann, C. G.; Radaelli, P. G.; Finney, J. L.; Mayer, E., *Phys. Chem. Chem. Phys.* **2008,** *10*, 6313-6324.
26. Rosu-Finsen, A.; Salzmann, C. G., *Chem. Sci.* **2019,** *10*, 515-523.

27. Komatsu, K.; Klotz, S.; Machida, S.; Sano-Furukawa, A.; Hattori, T.; Kagi, H., *Proc. Natl. Acad. Sci.* **2020**, *117*, 6356-6361.
28. Rosu-Finsen, A.; Amon, A.; Armstrong, J.; Fernandez-Alonso, F.; Salzmann, C. G., *J. Phys. Chem. Lett.* **2020**, *11*, 1106-1111.
29. Salzmann, C. G.; Rosu-Finsen, A.; Sharif, Z.; Radaelli, P. G.; Finney, J. L., *J. Chem. Phys.* **2021,** *154*, 134504.
30. Salzmann, C. G.; Mayer, E.; Hallbrucker, A., *Phys. Chem. Chem. Phys.* **2004**, *6*, 1269-1276.
31. Koster, K. W.; Fuentes-Landete, V.; Raidt, A.; Seidl, M.; Gainaru, C.; Loerting, T.; Bohmer, R., *Nat. Commun.* **2018,** *9*, 16189.
32. Pauling, L., *J. Am. Chem. Soc.* **1935,** *57*, 2680-2684.
33. Fuentes-Landete, V.; Köster, K. W.; Böhmer, R.; Loerting, T., *Phys. Chem. Chem. Phys.* **2018,** *20*, 21607-21616.
34. Handa, Y. P.; Klug, D. D.; Whalley, E., *J. Phys. Colloq.* **1987,** *48*, 435-440.
35. Minceva-Sukarova, B.; Slark, G.; Sherman, W. F., *J. Mol. Struct.* **1988,** *175*, 289-293.
36. Salzmann, C. G.; Hallbrucker, A.; Finney, J. L.; Mayer, E., *Phys. Chem. Chem. Phys.* **2006,** *8*, 3088-3093.
37. Salzmann, C. G.; Radaelli, P. G.; Hallbrucker, A.; Mayer, E.; Finney, J. L., *Science* **2006,** *311*, 1758-61.
38. Gasser, T. M.; Thoeny, A. V.; Plaga, L. J.; Köster, K. W.; Etter, M.; Böhmer, R.; Loerting, T., *Chem. Sci.* **2018,** *9*, 4224-4234.
39. Tuschel, D., *Spectroscopy* **2019,** *34*, 10-21.
40. Leadbetter, A. J.; Ward, R. C.; Clark, J. W.; Tucker, P. A.; Matsuo, T.; Suga, H., *J. Chem. Phys.* **1985,** *82*, 424-428.
41. Parkkinen, P.; Riikonen, S.; Halonen, L., *J. Phys. Chem. C* **2014,** *118*, 26264-26275.
42. Salzmann, C. G.; Radaelli, P. G.; Mayer, E.; Finney, J. L, *Phys. Rev. Lett.* **2009,** *103*, 105701.
43. Scherer, G. W., *Relaxation in Glass and Composites*. John Wiley & Sons: Corning, New York, 1986.
44. Salzmann, C. G.; Kohl, I.; Loerting, T.; Mayer, E.; Hallbrucker, A., *Phys. Chem. Chem. Phys.* **2003,** *5*, 3507-3517.